Published in final edited form as:
Birth Defects Res A Clin Mol Teratol. 2012 October ; 94(10): 782–789. doi:10.1002/bdra.23081.

Transcriptional Analyses of Two Mouse Models of Spina Bifida

Robert M. Cabrera[1], **Richard H. Finnell**[1,2], **Huiping Zhu**[1], **Gary M. Shaw**[3], and **Bogdan J. Wlodarczyk**[1,§]

[1]Department of Nutritional Sciences, Dell Pediatric Research Institute, The University of Texas at Austin, Austin, Texas

[2]Department of Chemistry and Biochemistry, The University of Texas at Austin, Austin, Texas

[3]Department of Pediatrics, Stanford University School of Medicine, Stanford, California

Abstract

Spina bifida is one of the most common of all human structural birth defects. Despite considerable effort over several decades, the causes and mechanisms underlying this malformation remain poorly characterized. In order to better understand the pathogenesis of this abnormality, we conducted a microarray study using Mouse Whole Genome Bioarrays which have ~36,000 gene targets, to compare gene expression profiles between two mouse models; *CXL-Splotch* and *Fkbp8*$^{Gt(neo)}$which express a similar spina bifida phenotype. We anticipated that there would be a collection of overlapping genes or shared genetic pathways at the molecular level indicative of a common mechanism underlying the pathogenesis of spina bifida during embryonic development.

A total of 54 genes were determined to be differentially expressed (25 down regulated, 29 upregulated) in the *Fkbp8Gt*$^{(neo)}$ mouse embryos; while 73 genes were differentially expressed (56 down regulated, 17 upregulated) in the *CXL-Splotch* mouse relative to their wildtype controls. Remarkably, the only two genes that showed decreased expression in both mutants were v-ski sarcoma viral oncogene homolog (*Ski*), and *Zic1,* a transcription factor member of the zinc finger family. Confirmation analysis using real time qRT-PCR indicated that only Zic1 was significantly decreased in both mutants. Gene Ontology analysis revealed striking enrichment of genes associated with mesoderm and central nervous system development in the *CXL-Splotch* mutant embryos, whereas in the *Fkbp8*$^{Gt(neo)}$ mutants, the genes involved in dorsal/ventral pattern formation, cell fate specification, and positive regulation of cell differentiation were most likely to be enriched. These results indicate that there are multiple pathways and gene networks perturbed in mouse embryos with shared phenotypes.

Keywords

spina bifida; gene expression; microarray; mouse mutants

Background

Neural tube defects (NTDs), one of the most common and severe of all human congenital malformations, are the result of defective neurulation and a failure of the early stage of brain and spinal cord formation during embryogenesis. These often lethal defects occur in human populations with a prevalence ranging from approximately 0.5 to 10 per 1,000 births, varying by country, geographical region, and ethnicity (Rosano et al., 2000; Canfield et al.,

§Corresponding author: Bogdan J. Wlodarczyk, The University of Texas at Austin, Department of Nutritional Sciences, Dell Pediatric Research Institute, 1400 Barbara Jordan Blvd., Austin TX 78723, bwlodarczyk@austin.utexas.edu, phone: 512-495-3002, fax: 512-495-4805.

2006; Boulet et al., 2008). The most frequent forms of NTDs are anencephaly, a malformation characterized by the absence of cranial vault with the brain missing or greatly reduced, and spina bifida, a malformation of the spinal column characterized by herniation or exposure of the spinal cord through incompletely closed vertebras. Several studies have demonstrated that isolated NTDs have a multifactorial origin, with significant contributions from both genetic and environmental factors (Campbell et al., 1986; Finnell et al., 2000; Deak et al., 2008). However, despite years of epidemiological and experimental studies, the mechanism responsible for NTDs remains largely unknown.

To elucidate mechanisms underlying the etiology of neural tube closure defects, different experimental models have been extensively exploited. Mouse embryos have been one of the most often used models, especially spontaneous and genetically modified mouse mutants that exhibit NTD phenotypes. There are a large number of spontaneous and transgenic mutant mice presenting with cranial (exencephaly) or spinal (spina bifida) defects (Green and Copp, 2005). More recently, by applying genetic engineering techniques, new murine NTD models have been created. Inactivation of genes involved in the neurulation process resulted in establishing knockout mice exhibiting NTDs (Juriloff and Harris, 2000; Zohn et al., 2005; Harris and Juriloff, 2010).

The *Fkbp8* gene belongs to a family of immunophilin FK506-binding proteins functioning in immunoregulation, protein folding and trafficking. FKBP8 is a 44 kDa mitochondrial protein which has three tetratricopeptide repeat (TPR) motifs, which are protein-protein interaction domains that mediate physical associations between FKBP8 and its protein interactors. The N-terminus of FKBP8 contains a peptidylprolyl cis-trans isomerase (PPIase) domain that is conserved throughout the FKBP family, and it is important for FK506 binding and PPIase activity (Moore et al., 1991). *In vitro* studies have shown that FKBP8 controls apoptosis by binding BCL-2, promoting its stability, and targeting this anti-apoptotic factor to the mitochondria. FKBP8 primarily acts in a cell-autonomous fashion to prevent inappropriate activation of the Hedgehog pathway by GLI2. Disruption of *Fkbp8* affects neural patterning by changing the signaling environment of neural progenitors (Cho et al., 2008). The *Fkbp8* gene had been previously targeted in the mouse where a neo cassette was inserted to disrupt part of the PPIase and TPR domains (Bulgakov et al. 2004). Homozygous mutants displayed posterior neural tube, dorsal root ganglion and optic defects, but the mutation was embryolethal by E13.5. The $Fkbp8^{Gt(neo)}$ knockout mouse is a new model of posterior NTDs. These mutant mice created by gene-trapping, survive to term like the *CXL-Sp*, and all of the mice present with 100% penetrant spina bifida (Wong et al., 2008).

Splotch is a mouse mutant that has been used by investigators as a model system for the study of NTDs for more than 60 years. These mice carry semidominant mutations in the transcription factor *Pax3*, which arose spontaneously in the C57BL/6J mouse strain (Douglass and Russell, 1947). In embryos that are homozygous (*Sp/Sp*), the splotch mutation results in multiple malformations including those of the nervous system (spina bifida with or without exencephaly, reduced or absent spinal ganglia, deficiency of Schwann cells), cardiovascular system (cardiac malformations involving partial or complete failure of septation of the outflow tract, so called conotruncal heart defects), skin (absence of melanocytes), and muscles (reduced axial muscles along a rostro-caudal gradient and slower development of limb muscles) (Auerbach, 1954; Franz et al., 1993; Epstein et al., 2000). The homozygous *Sp/Sp* embryos die *in utero* by E14. *Splotch* heterozygotes (*Sp/+*) are viable and exhibit a pigmentation defect that presents as a white belly spot, sometimes extending to the limbs and tail. The white spots result from the failure of neural crest cell-derived melanocytes migrating into these regions.

Several alleles of splotch have been identified (*Sp, Sp^{J}, Sp^{2J}, Sp^{3J}, Sp^{d}, Sp^{r}, Sp^{1H}, Sp^{2H}, Sp^{4H}*), and all of them harbor mutations in the *Pax3* gene, which has been mapped to mouse chromosome 1 (Dickie, 1964; Epstein et al., 1991; Goulding and Paquette, 1994). *Pax3* is a member of a highly conserved, paired-box containing transcription factor gene family (Chi and Epstein, 2002). *Pax* genes are expressed in various organs and tissues in the developing embryo, and being multifunctional, they play critical roles in cell fate determination, survival, and proliferation. In general, *Pax* gene expression diminishes during the later stages of development in parallel with definitive differentiation. In the mouse embryo, *Pax3* is expressed by pre-migratory neural crest cells and by presomitic mesoderm as early as E8.5, and over time becoming increasingly restricted to the dorsal neural tube, where neural crest cells are specified, and to the maturing somites (Goulding et al., 1991). Neural crest cells are multipotent migratory cells that give rise to several of the tissues contributing to the peripheral nervous system, enteric ganglia, melanocytes, vascular smooth muscle, skeletal muscle, bone and cartilage of the face, and to a range of other cell types. *Pax3* plays a critical role during development of many neural crest derivatives (Stuart et al., 1994).

In this study, we used the highly inbred *CXL-Splotch* mouse strain, which originated from crosses between the C57BL/J6-Sp and LM/Bc/Fnn inbred strains (Gefrides et al., 2002). We sequenced the fragment of *CXL-Sp Pax3* gene covering 3′ extremity of intron 3 and the 5′ extremity of exon 4, and the splotch mutation was confirmed to be identical to the spontaneous *Sp* mutation described by Epstein et al. (1993). Unlike most *Splotch* mutant homozygotes that die between E12 and E14, the *CXL-Sp Pax3* homozygotes often survive to term.

In our previous studies, we demonstrated that *CXL-Splotch* mutant mice at E18.5 present with severe spina bifida located in the lumbo-sacral region. This location suggests that the pathogenesis involve disrupted closure of posterior neuropore, a mechanism observed also in other Splotch mutants (Yang and Trasler, 1991). The spina bifida lesion observed in $Fkbp8^{Gt(neo)}$ is also predominantly located in the lumbo-sacral region; however, it often extends into the lower thoracic area. Morphological study suggests that this defect is the result of a dilation of the neural tube, rather than problems with closing and fusion of the NT (Wong et al., 2008). Both the $Fkbp8^{Gt(neo)}$ and *CXL-Splotch* mutant mice, despite multiple morphological differences, consistently present with the shared common feature of a posterior NTD. These severe perturbations in the process of spinal cord development and that of surrounding tissue formation, although originating from the mutation of different genes (*Pax3* and *Fkbp8*), lead to a phenotypically similar spina bifida malformation in the affected mice. In order to elucidate the mechanism of spina bifida formation, we examined gene expression patterns in the posterior neural tube and surrounding tissue of embryos from these two mouse models. To determine whether any similarities exist in the gene expression patterns and to identify shared genes and pathways that are altered in these two genetically distinct mouse models of NTDs, we initially compared the gene expression patterns in the wildtype embryos with that of the respective homozygous mutants samples for each of the mouse models, then we compared the samples from $Fkbp8^{Gt(neo)}$ and *CXL-Splotch* homozygotes to each other. We anticipated that despite the obvious genetic differences in these two NTD mutants, we would discover a collection of overlapping genes or pathways that might reveal at a molecular level a common mechanism underlying the formation of spina bifida during murine development.

Methods

Collection of $Fkbp8^{Gt(neo)}$ and CXL-Splotch embryos

All animal experiments were reviewed and approved by the Institutional Animal Care and Use Committee (IACUC) of the Texas A&M Health Science Center Institute of Biosciences

and Technology (IBT). The heterozygous *Fkbp8*$^{Gt(neo)}$ (*Fkbp8*$^{+/-}$) and heterozygous *CXL-Splotch* (*Sp/+*) mice were housed in the IBT Vivarium. The animals were maintained in clear polycarbonate microisolator cages and were allowed free access to food and water (Harlan Teklad Rodent Diet #8606, Ralston Purina, St. Louis MO) and were maintained on a 12-h light/dark cycle. Virgin (*Fkbp8*$^{+/-}$ and *Sp/+* females, 50– 70 days of age, were mated overnight with (*Fkbp8*$^{+/-}$ and *Sp/+*, respectively) males and examined for the presence of vaginal plugs the following morning. The onset of gestation was set at 10 p.m. of the previous night, the midpoint of the dark cycle. Pregnant females were sacrificed at embryonic day 9 plus 12 hours (E 9.5), the abdomen opened and uteri removed and placed in a Petri dish filled with DEPC PBS. The uterus was cut opened and the embryos in their deciduas moved to ice-cold DEPC PBS. Under the dissecting microscope, the embryos were carefully freed from the decidual and embryonic membranes, and were grossly examined in order to stage the embryos according to their number of somites and their individual advancement through the process of neural tube closure. A total of 26 embryos were harvested from four *Fkbp8*$^{+/-}$ females and 47 embryos were collected from six *Sp/+* females. At E 9.5, the typical embryo was “C”-shaped and had 21.6 and 21.3 (*Fkbp8*$^{Gt(neo)}$ and *CXL-Splotch,* respectively) pairs of somites and neural tube closure was complete with the exception of the posterior neuropore. At this stage of development (E9.5), there were no visible morphological differences between wild type, heterozygous and homozygous embryos in the *Fkbp8* knockout and *Splotch* mutants. For the microarray assay, the posterior part of the embryo (immediately below the forelimb bud) was cut off and transferred separately to a 600μl plastic tube containing 15μl of RNAlater (Ambion). The samples were placed in 4°C for 24 h, and then transferred and stored frozen at −80°C until further processed. The remaining anterior part of the embryo was transferred to 1.5 ml tube and stored at −20°C until they were processed for genomic DNA extraction and subsequent genotyping, as described previously (Wlodarczyk et al., 2006; Wong et al., 2008).

Total RNA was extracted from the harvested posterior portions of E9.5 embryos using a PicoPure RNA isolation Kit (Arcturus). To prevent contamination with DNA, the RNA was treated with DNase prior to the final elution from the purification column. From the 20μl of eluted RNA, 1μl was used for the concentration analysis with a NanoDrop ND-1000 spectrophotometer. The amount of total RNA extracted from the posterior portion of E9.5 embryos was in the range of 3-7μg, with an average 3.4 μg for *Fkbp8*$^{Gt(neo)}$ and 3.6 μg for *CXL-Splotch*. Additionally, the RNA quality was assessed on an Agilent 2100 Bioanalyzer using Pico LabChips (Agilent). Undegraded RNA from six *Fkbp8*$^{Gt(neo)}$ embryos [three wild type (*Fkbp8*$^{+/+}$) and three *Fkbp8*$^{-/-}$] and six *CXL-Splotch* embryos [three wild type (*+/+*) and three homozygous *Sp/Sp*] were processed by the Genomic Core of the Texas A&M University for microarray analysis. RNA samples were selected from embryos (*Fkbp8*$^{+/+}$ versus *Fkbp8*$^{-/-}$, *+/+* versus *Sp/Sp*) that originated from a single dam for microarray processing.

Microarray assay

RNA that has passed the Agilent Technologies 2100 Bioanalyzer quality control test was used to generate biotin-labeled cRNA via a modified Eberwine RNA amplification protocol (Eberwine et al., 1992). Labeled cRNA was applied to the bioarray and incubated for 18 hours. Following the incubation period, the slide batch was processed and then scanned using an Agilent DNA Microarray Scanner.

The cRNA samples were hybridized to CodeLink Mouse Whole Genome Bioarray (Applied Microarrays), which contain ~36,000 mouse gene targets. The probe sequences, representing well annotated, full-length and partial mouse gene sequences, were designed based on data from the NCBI UniGene build #139, RefSeq database, and dbEST database. The gene

expression data were deposited into the NCBI Gene Expression Omnibus website (http://www.ncbi.nlm.nih.gov/geo), and can be accessed via accession number GSE25983.

Microarray data analysis

Initial feature extraction from the images was performed using CodeLink Expression Analysis software v4.0 (GE Healthcare, Piscataway, NJ). Intensities for individual genes were determined by the median intensity of all pixels within the spot's region. Array data was subject to grand-median normalization. Thresholds were set using negative control gene probes (Raf). Average signal and standard deviations were determined for negative probes, and signal thresholds were set at three standard deviations above average negative control signals. For each experiment, at least two of the three gene probes were required to pass threshold for inclusion in the analysis. This threshold was set to eliminate very weakly expressed genes. Criteria for differential expression were set as 1) >2 fold increase/decrease in median gene expression between experimental and controls; 2) >1.25 for the absolute median fold change ($\log_2$) multiplied by the absolute difference (δ) between median control and median experimental values. Due to relatively low number of samples (N=12), stratified further to two different mutant strains (*Fkbp8*$^{Gt(neo)}$ and *CXL-Splotch*), each consisting of two genotype (wild type and homozygous mutant), the microarray data was analyzed for significant enrichment of gene ontology groups. This effectively reduced the number of multiple comparisons; producing only lists of genes with changes in gene expression of significantly enriched gene ontology groups. P-values were adjusted using multiple test adjustment (Benjamini and Hochberg, 1995). qRT-PCR was performed in order to validate the microarray results for selected genes.

Quantitative Real Time PCR

For this purpose, RNA was extracted from new *Fkbp8* and *Splotch* embryos (both wild type and homozygous mutants) using the same method as for the microarray assay. Differentially expressed genes (based on the microarray results) were categorized using " Web Gestalt " Gene Set Analysis Tookit V2 (http://bioinfo.vanderbilt.edu/webgestalt); eight of these genes were selected for the validation assay. TaqMan® Gene Expression Assays were used to evaluate gene expression changes for these selected genes. Gene-specific probes and primer sets were purchased from Applied Biosystems (Foster City, CA). The RNA was reverse transcribed to cDNA and 50ng of each sample was mixed with 10μl TaqMan® Gene Expression PCR Master Mix (Applied Biosystems, Foster City, CA) and 1 μl probe and primer mixture in a total volume of 20 μl in a 384-well plate. The assays were performed according to manufacturer's protocol on an ABI PRISM® 7900HT Sequence Detection System (Applied Biosystems, Foster City, CA). The thermo-cycling started with a 10 min denaturing at 95°C, followed by 40 cycles of 95°C for 15sec and 60°C for 1 min. Data was analyzed using SDS software v2.1 (Applied Biosystems, Foster City, CA). Mouse *Gapdh* gene was used as internal control. $\Delta\Delta C_T$ method was used to generate relative quantitative values (fold change). T-test was used to compute the p-values for ΔC_T between different genotypes. At least 4 samples were used for each genotype. Each reaction was replicated 2 times and the mean value was used in final comparisons.

Neural tube defects

The *CXL-Splotch* homozygous mice used in this study survive to term. We have observed several of the pups to be live born with spina bifida (Fig. 2). In all cases, the lesion was localized to the lumbo-sacral region and consisted of exposed, dysplastic spinal cord protruding with or without meninges throughout opened vertebral dorsal arches. A thin, translucent skin layer covering this lesion usually was ruptured during the delivery process or shortly thereafter.

The *Fkbp8*$^{Gt(neo)}$ knockout mouse used was not embryo lethal, resulting in 100% penetrant affected live born pups. This homozygous mutant displays similar morphological features, including cystic protrusion at the thoracico-lumbo-scaral region (often ruptured at birth); with a dysplastic spinal cord (Fig. 3) and vertebral arches that failed to fuse at the dorsal midline, as well as lower body paralysis (Wong et al., 2008).

Results

Microarray Results

The threshold applied to the microarray data eliminated approximately 95% of low expressing genes that pass the threshold for absolute fold changes (*e.g.* $\log_2$ ratio > 1), but showed relatively small changes in absolute values (*e.g.* δ < 1.25) (Figure 1). A total of 55 genes were determined to be differentially expressed (26 down- and, 29 up-regulated) in the *Fkbp8*$^{Gt(neo)}$ embryos. In the *CXL-Splotch* arrays, a total of 73 genes were determined to be differentially expressed (56 down, 17 up). These genes were further sub-categorized into Gene Ontology (GO) terms using Gene Set Analysis Tookit V2 (Zhang et al., 2003, 2004), which identified enrichment of genes associated with mesoderm development (GO: 0007498) and central nervous system development (GO:0007417) in *CXL*-Splotch and dorsal/ventral pattern formation and cell fate specification and positive regulation of cell differentiation in *Fkbp8*$^{Gt(neo)}$ (Table 1). The mesoderm GO consists of genes that function in the development and differentation of mesoderm structures. This is related to both mutants, since somite are defined as mesoderm. The somites further differentiate into sclerotome (bone), myotome (muscles), and dermatome (skin), all of which are disrupted in these mouse models of NTDs. The CNS development group consists of genes that control the processes of development and formation of the CNS. Microarray results identified two genes, v-ski sarcoma viral oncogene homolog (*Ski*) and *Zic1*, which showed decreased expression in both *CXL-Splotch* and *Fkbp8*$^{Gt(neo)}$ microarrays (Table 2 and Figure 4).

Discussion

We hypothesized that *Fkbp8*$^{Gt(neo)}$ and *CXL-Splotch* mice would share common gene expression patterns given the fact that comparable embryonic tissues were collected from mutant embryos of the two genotypes, and the fact that both mutants presented with a common phenotype, namely posterior neural tube defect. However, the molecular cascades that appear to influence this shared abnormal phenotype differ, and these differences were evident in the altered gene expression patterns and gene ontologies observed. Specifically, in *CXL-Splotch* mutant, genes differentially expressed were associated with mesoderm development (Table 1. GO:0007498). This was expected, based on previously published reports of the early mesodermal phenotypes observed in *Splotch* mutant epithelial somites (Schubert et al., 2001). The genes identified in this region by ontology group (Table 1, *Epb4.1l5, Osr1, Lhx2*) are expected to function downstream of Splotch based on spatial and temporal relationships between these genes during mesoderm development. Specifically, the FERM-domain gene erythrocyte protein band 4.1-like 5 (*Epb4.1l5*), also called *Lulu*, has been shown to affect epithelial-mesenchymal transition, such that *Lulu* nullizygous embryos have reduced paraxial mesoderm (Lee et al., 2007), where Pax3 is also a marker for neural crest (Goulding et al., 1991). The Odd-skipped related 1 gene (*Osr1*) has also been reported to influence the formation and differentiation of paraxial mesoderm into kidney precursor cells (James et al., 2006). While kidney tubule defects have not been reported in *Splotch* mice, clinical reports of *Waardenburg* syndrome have indicated the presence of rare renal anomalies in some patients (Kaplan and de Chaderevian, 1988; Jankauskiene et al., 1997; Ekinci et al. 2005). *Sox10* was also differentially expressed in the posterior region of the neural tube of *Splotch* mice (Table 2). The SOX10 protein modulates other transcription factors, including *Pax3*, and belongs to the high mobility group (HMG) box superfamily of

DNA-binding proteins. *Sox10, Pax3, Creb* and *Lef1* are all transcription factors that control *Mitf* expression. *Splotch* mutant carriers also display alterations in pigmentation, and the expression of *Sox10* in the *Splotch* embryos may influence not only the neural crest in the posterior neural tube but also the migration of neural crest derived melanoblasts to the region of hypopigmentation on *Splotch* mutants.

FKBP8 is a member of the immunophilins family, which are a conserved family of cis trans peptidyl-prolyl isomerases. FKBP8 has been reported to function as an antagonist of Hedgehog signaling in the caudal neural tube (Bulgakov et al., 2004). Loss of FKBP8 activity leads to an expansion of the floor plate and ventral neural cells as well as altered cells identity along the dorso-ventral axis, which ultimately leads to the observed posterior neural tube defect in the $Fkbp8^{Gt(neo)}$ homozygotes. This phenotype indicates that the activity is specific to the posterior region of the neural tube (Figure 3). The gene expression data obtained from the $Fkbp8^{Gt(neo)}$ embryos indicated that the Dorsal/Ventral Pattern Formation (GO:0009953) group was significantly altered (Table 1). The genes reported in this GO included *Hoxd11* and *Foxa2* being upregulated, and *Dbx1* and *Fkbp8* being down-regulated. Such data are expected to impact $Fkbp8^{Gt(neo)}$ mutants in several distinct ways. Specifically, during spinal cord development, distinct classes of inter-neurons are generated from progenitor cells located at different positions within the ventral neural tube. The V0 and V1 inter-neurons derive from adjacent progenitor domains that are distinguished by expression of the homeodomain proteins, DBX1 and DBX2. The spatial expression of DBX1 has a critical role in establishing the distinction in V0 and V1 neuronal fate. In *Dbx1* mutant mice, neural progenitors fail to generate V0 neurons (Pierani et al., 2001). If altered expression in *Dbx1* (differentially expressed, Table 1 & 2) due to $Fkbp8^{Gt(neo)}$ produces similar developmental consequences, *Fkbp8* may also influence V0 and V1 neuronal fate. Additionally, the *Foxa* transcription factors comprise a subfamily of forkhead transcription factors that are known to have important roles in notochord, neural tube, and gut tube formation (Weinstein et al., 1994). The observed increase in *Foxa2* expression (Table 1 and 2) is also reported and explained by previous observation of expansion of *Foxa2* in the $Fkbp8^{-/-}$ mutants, where the ventral half of the neural tube expressed this marker [25]. *Foxa2* also impacts adipocyte differentiation and has been reported by Wolfrum et al. (2003) to act as a transcriptional activator of *lipoprotein lipase* (*Lpl*). Consistent with this report, overexpression of *Foxa2* coincided with activation of *Lpl* (fold change 1.1) in the posterior neural tube tissues of $Fkbp8^{-/-}$ mutants.

Adenosine deaminase (ADA) is a catabolic enzyme that modifies levels of adenosine and 2′-deoxyadenosine in cells. It was observed to be differentially over-expressed in *Fkbp8* mutants (fold change 2.51). Genetic deficiencies in *Ada* in mouse and human are notable in producing severe lymphopenia and immunodeficiency (Blackburn et al., 2000). Neural tube closure still proceeds in the absence of *Ada*, as indicated by mutant models that die perinatally with hepatocellular impairment (Wakammiya et al., 1995). The impact of over-expression of *Ada* on adenosine catabolism in *Fkbp8* mutants is expected to influence neuronal differentiation in neural crest cells (Bilodeau et al., 2005).

We initially identified *Ski*, an oncogene present in the avian Sloan-Kettering viruses, as the only gene to be differentially expressed in the microarray data from both mutant models. However, qRT-PCR results (Table 2, p=0.52) did not confirm that *Ski* was significantly down-regulated in *CXL-Splotch* embryos. The data from the microarray and qRT-PCR were similar, such that the up-regulation or down regulation of the gene was consistent with qRT-PCR results (9 out of 10 genes), but these observed changes did not always reach significant levels by qRT-PCR ($P<0.05$, for 5 out of 10 genes). *Zic1* was found to be significantly down regulated in both the *Sp/Sp* and $Fkbp8^{-/-}$ embryos (Table 2). *Zic* genes are vertebrate homologs of odd-paired, the Drosophila pair-rule gene, and have an essential role in neural

development. Specifically, ZIC proteins function as transcriptional regulators in hedgehog signaling. Recent studies of numerous model systems has demonstrated that *Zic* influence neurogenesis, myogenesis, skeletal patterning, and left-right axis establishment. Their influence on neural development includes controlling the initial phase of ectoderm differentiation into neuroectoderm. Mutations in *Zic* family genes often result in neural tube defects, which are seen at different rostrocaudal levels depending on which *Zic* gene subtype has been affected (Carrel et al., 2001; Inoue et al., 2004). The ZIC proteins can also inhibit neuronal differentiation by activating *Notch* signals (Aruga, 2004). In the models investigated in this study, the decreased expression in *Zic* family genes occurs in parallel and may partially explain the production of NTDs in homozygous mutant *CXL-Splotch* and *Fkbp8*$^{-/-}$ mice. Specifically, the convergence on *Zic1* gene expression in the posterior dorsal neural tube is expected to influence neural differentiation in the area. If this decrease in expression is coupled to a decrease in dorsal ventricular cell mass, both models would be expected to induce premature neuronal differentiation (Aruga et al., 2002). *Zic* genes also function as *Gli* co-factors in Hedgehog signaling (Pan et al., 2011). The expression pattern of *Zic1* is altered in the absence of SHH (Fogel et al., 2008). SHH signaling is affected in several NTD mouse models such as mice with knocked out planar cell polarity (PCP) effector gene, *Fuz* (Gray et al., 2009). Altered Zic1 expression may contribute to abnormal neural tube closure in animals with disrupted PCP signaling.

Human studies have failed to establish an association between *ZIC* family gene mutations and risk for NTDs (Klootwijk et al., 2004); however, reduction of *Zic 1* expression is associated with teratogen-induced NTDs and alterations of gene expression in mice (Robinson et al., 2009). Analyses of *Ski* mutations in mice have demonstrated induction of midline facial clefting and NTDs, and human studies have indicated *SKI* is deleted in all of the individuals tested with 1p36 deletion syndrome (Colmenares et al., 2002). Therefore, we suggest that the analysis of the genes identified in this study may prove useful for association analysis for polymorphisms as NTD risk factors in humans. Using these data to guide functional genomics (i.e. gene expression) studies in humans may provide greater benefit but would also require a sample collection challenge to obtain whole tissues and isolated cells for RNA and DNA isolation from an embryonic relevant time period. We look forward to testing both of these scenarios in future studies.

Acknowledgments

The authors would like to thank Hui Wei for her excellent assistance with Fkbp8 genotyping, and acknowledge the support of NIH grants DE016315 to RHF and NS050249 to GMS.

This study was supported by National Institutes of Health grants DE016315 to RHF and NS050249 to GMS.

References

1. Aruga J. The role of Zic genes in neural development. Mol Cell Neurosci. 2004; 26(2):205–221. [PubMed: 15207846]
2. Aruga J, Tohmonda T, Homma S, Mikoshiba K. Zic1 promotes the expansion of dorsal neural progenitors in spinal cord by inhibiting neuronal differentiation. Dev Biol. 2002; 244(2):329–341. [PubMed: 11944941]
3. Auerbach R. Analysis of developmental effects of a lethal mutation in a house mouse. J Exp Zool. 1954; 127:305–327.
4. Benjamini Y, Hochberg Y. Controlling the false discovery rate: a practical and powerful approach to multiple testing. J Roy Statist Soc Ser B (Methodological). 1995; 57:289–300.
5. Bilodeau ML, Ji M, Paris M, Andrisani OM. Adenosine signaling promotes neuronal, catecholaminergic differentiation of primary neural crest cells and CNS-derived CAD cells. Mol Cell Neurosci. 2005; 29(3):394–404. [PubMed: 15886017]

6. Blackburn MR, Volmer JB, Thrasher JL, Zhong H, Crosby JR, Lee JJ, Kellems RE. Metabolic consequences of adenosine deaminase deficiency in mice are associated with defects in alveogenesis, pulmonary inflammation, and airway obstruction. J Exp Med. 2000; 192(2):159–70. [PubMed: 10899903]

7. Boulet SL, Yang Q, Mai C, Kirby RS, Collins JS, Robbins JM, Meyer R, Canfield MA, Mulinare J. Trends in the postfortification prevalence of spina bifida and anencephaly in the United States. Birth Defects Res A Clin Mol Teratol. 2008; 82(7):527–532. [PubMed: 18481813]

8. Bulgakov OV, Eggenschwiler JT, Hong DH, Anderson KV, Li T. FKBP8 is a negative regulator of mouse sonic hedgehog signalling in neural tissues. Development. 2004; 131(9):2149–2159. [PubMed: 15105374]

9. Campbell LR, Dayton DH, Sohal GS. Neural tube defects: a review of human and animal studies on the etiology of neural tube defects. Teratology. 1986; 34(2):171–187. [PubMed: 3535149]

10. Canfield MA, Honein MA, Yuskiv N, Xing J, Mai CT, Collins JS, Devine O, Petrini J, Ramadhani TA, Hobbs CA, et al. National estimates and race/ethnic-specific variation of selected birth defects in the United States, 1999-2001. Birth Defects Res A Clin Mol Teratol. 2006; 76(11):747–756. [PubMed: 17051527]

11. Carrel T, Herman GE, Moore GE, Stanier P. Lack of mutations in ZIC3 in three families with neural tube defects. American Journal of Medical Genetics. 2001; 98:283–285. [PubMed: 11169570]

12. Chi N, Epstein JA. Getting your Pax straight: Pax proteins in development and disease. Trends Genet. 2002; 18(1):41–7. [PubMed: 11750700]

13. Cho A, Ko HW. FKBP8 cell-autonomously controls neural tube patterning through a Gli2- and Kif3a-dependent mechanism. Developmental Biology. 2008; 321:27–39. [PubMed: 18590716]

14. Colmenares C, Heilstedt HA, Shaffer LG, Schwartz S, Berk M, Murray JC, Stavnezer E. Loss of the SKI proto-oncogene in individuals affected with 1p36 deletion syndrome is predicted by strain-dependent defects in $Ski^{-/-}$ mice. Nat Genet. 2002; 30(1):106–9. [PubMed: 11731796]

15. Deak KL, Siegel DG, George TM, Gregory S, Ashley-Koch A, Speer MC. Further evidence for a maternal genetic effect and a sex-influenced effect contributing to risk for human neural tube defects. Birth Defects Res A Clin Mol Teratol. 2008; 82(10):662–669. [PubMed: 18937341]

16. Dickie MM. New splotch alleles in the mouse. J Hered. 1964; 55:97–101. [PubMed: 14170406]

17. Epstein DJ, Vekemans M, Gros P. Splotch (Sp2H), a mutation affecting development of the mouse neural tube, shows a deletion within the paired homeodomain of Pax-3. Cell. 1991; 67(4):767–774. [PubMed: 1682057]

18. Douglass P, Russell WL. A histological study of eye abnormalities in the C57 black strain of mice. Anat Rec. 1947; 97(3):414. [PubMed: 20290931]

19. Eberwine J, Spencer C, Miyashiro K, Mackler S, Finnell R. Complementary DNA synthesis in situ: methods and applications. Methods Enzymol. 1992; 216:80–100. [PubMed: 1479921]

20. Ekinci S, Ciftci AO, Senocak ME, Buyukpamukcu N. Waardenburg syndrome associated with bilateral renal anomaly. J Pediatr Surg. 2005; 40(5):879–881. [PubMed: 15937838]

21. Epstein DJ, Vogan KJ, Trasler DG, Gros P. A mutation within intron 3 of the Pax-3 gene produces aberrantly spliced mRNA transcript in the splotch (Sp) mouse mutant. Proc Natl Acad Sci USA. 1993; 90:532–536. [PubMed: 8421686]

22. Epstein JA, Li J, Lang D, Chen F, Brown CB, Jin F, Lu MM, Thomas M, Liu E, Wessels A, Lo CW. Migration of Cardiac neural crest cell in splotch embryos. Development. 2000; 127(9):1869–1878. [PubMed: 10751175]

23. Finnell RH, Gelineau-van Waes J, Bennett GD, Barber RC, Wlodarczyk B, Shaw GM, Lammer EJ, Piedrahita JA, Eberwine JH. Genetic basis of susceptibility to environmentally induced neural tube defects. Ann N Y Acad Sci. 2000; 919:261–277. [PubMed: 11083116]

24. Fogel JL, Chiang C, Huang X, Agarwala S. Ventral specification and perturbed boundary formation in the mouse midbrain in the absence of Hedgehog signaling. Dev Dyn. 2008; 237(5): 1359–1372. [PubMed: 18429041]

25. Franz T, Kothary R, Surani MA, Halata Z, Grim M. The Splotch mutation interferes with muscle development in the limbs. Anat. Embryol. 1993; 187(2):153–160. [PubMed: 8238963]

26. Gefrides LA, Bennett GD, Finnell RH. Effect of folate supplementation on the risk of spontaneous and induced neural tube defects in splotch mice. Teratology. 2002; 65:63–69. [PubMed: 11857507]
27. Goulding MD, Chalepakis G, Deutsch U, Erselius JR, Gruss P. Pax-3, a novel murine DNA binding protein expressed during early neurogenesis. EMBO J. 1991; 10(5):1135–47. [PubMed: 2022185]
28. Goulding, M.; Paquette, A. Pax genes and neural tube defects in the mouse; the Ciba Foundation Symposium; Neural tube defects, Wiley, Chichester. 1994; p. 103-117.
29. Gray RS, Abitua PB, Wlodarczyk BJ, Szabo-Rogers HL, Blanchard O, Lee I, Weiss GS, Liu KJ, Marcotte EM, Wallingford JB, Finnell RH. The planar cell polarity effector Fuz is essential for targeted membrane trafficking, ciliogenesis and mouse embryonic development. Nat Cell Biol. 2009; 11(10):1225–1232. [PubMed: 19767740]
30. Greene ND, Copp AJ. Mouse models of neural tube defects: investigating preventive mechanisms. Am J Med Genet C Semin Med Genet. 2005; 135(1):31–41. [PubMed: 15800852]
31. Harris MJ, Juriloff DM. An update to the list of mouse mutants with neural tube closure defects and advances toward a complete genetic perspective of neural tube closure. Birth Defects Res A Clin Mol Teratol. 2010; 88(8):653–69. [PubMed: 20740593]
32. Inoue T, Hatayama M, Tohmonda T, Itohara S, Aruga J, Mikoshiba K. Mouse Zic5 deficiency results in neural tube defects and hypoplasia of cephalic neural crest derivatives. Dev Biol. 2004; 270(1):146–162. [PubMed: 15136147]
33. James RG, Kamei CN, Wang Q, Jiang R, Schultheiss TM. Odd-skipped related 1 is required for development of the metanephric kidney and regulates formation and differentiation of kidney precursor cells. Development. 2006; 133(15):2995–3004. [PubMed: 16790474]
34. Jankauskiene A, Dodat H, Deiber M, Rosenberg D, Cochat P. Multicystic dysplastic kidney associated with Waardenburg syndrome type 1. Pediatr Nephrol. 1997; 11(6):744–745. [PubMed: 9438657]
35. Juriloff DM, Harris MJ. Mouse models for neural tube closure defects. Hum Mol Genet. 2000; 9(6):993–1000. [PubMed: 10767323]
36. Kaplan P, de Chaderevian JP. Piebaldism-Waardenburg syndrome: histopathologic evidence for a neural crest syndrome. Am J Med Genet. 1988; 31(3):679–688. [PubMed: 3228147]
37. Klootwijk R, Groenen P, Schijvenaars M, Hol F, Hamel B, Straatman H, Steegers-Theunissen R, Mariman E, Franke B. Genetic variants in ZIC1, ZIC2, and ZIC3 are not major risk factors for neural tube defects in humans. Am J Med Genet A. 2004; 124 A(1):40–7. [PubMed: 14679585]
38. Lee JD, Silva-Gagliardi NF, Tepass U, McGlade CJ, Anderson KV. The FERM protein Epb4.1l5 is required for organization of the neural plate and for the epithelial-mesenchymal transition at the primitive streak of the mouse embryo. Development. 2007; 134(11):2007–2016. [PubMed: 17507402]
39. Moore JM, Peattie DA, Fitzgibbon MJ, Thomson JA. Solution structure of the major binding protein for the immunosuppressant FK506. Nature. 1991; 351:248–250. [PubMed: 2041572]
40. Pan H, Gustafsson MK, Aruga J, Tiedken JJ, Chen JC, Emerson CP. A role for Zic1 and Zic2 in Myf5 regulation and somite myogenesis. Dev Biol. 2011; 351(1):120–127. [PubMed: 21211521]
41. Pierani A, Moran-Rivard L, Sunshine MJ, Littman DR, Goulding M, Jessell TM. Control of interneuron fate in the developing spinal cord by the progenitor homeodomain protein Dbx1. Neuron. 2001; 29(2):367–384. [PubMed: 11239429]
42. Robinson JF, Yu X, Hong S, Griffith WC, Beyer R, Kim E, Faustman EM. Cadmium-induced differential toxicogenomic response in resistant and sensitive mouse strains undergoing neurulation. Toxicol Sci. 2009; 107(1):206–19. [PubMed: 18974090]
43. Rosano A, Botto LD, Botting B, Mastroiacovo P. Infant mortality and congenital anomalies from 1950 to 1994: an international perspective. J Epidemiol Community Health. 2000; 54(9):660–666. [PubMed: 10942444]
44. Schubert FR, Tremblay P, Mansouri A, Faisst AM, Kammandel B, Lumsden A, Gruss P, Dietrich S. Early mesodermal phenotypes in splotch suggest a role for Pax3 in the formation of epithelial somites. Dev Dyn. 2001; 222(3):506–521. [PubMed: 11747084]

45. Stuart ET, Kioussi C, Gruss P. Mammalian Pax genes. Annu Rev Genet. 1994; 28:219–36. [PubMed: 7893124]
46. Wakamiya M, Blackburn MR, Jurecic R, McArthur MJ, Geske RS, Cartwright J Jr, Mitani K, Vaishnav S, Belmont JW, Kellems RE, et al. Disruption of the adenosine deaminase gene causes hepatocellular impairment and perinatal lethality in mice. Proc Natl Acad Sci USA. 1995; 92(9): 3673–7. [PubMed: 7731963]
47. Weinstein DC, Ruiz i Altaba A, Chen WS, Hoodless P, Prezioso VR, Jessell TM, Darnell JE Jr. The winged-helix transcription factor HNF-3 beta is required for notochord development in the mouse embryo. Cell. 1994; 78(4):575–588. [PubMed: 8069910]
48. Wlodarczyk BJ, Tang LS, Triplett A, Aleman F, Finnell RH. Spontaneous neural tube defects in splotch mice supplemented with selected micronutrients. Toxicol Appl Pharmacol. 2006; 213(1): 55–63. [PubMed: 16226775]
49. Wolfrum C, Shih DQ, Kuwajima S, Norris AW, Kahn CR, Stoffel M. Role of Foxa-2 in adipocyte metabolism and differentiation. J Clin Invest. 2003; 112(3):345–56. [PubMed: 12865419]
50. Wong RL, Wlodarczyk BJ, Min KS, Scott ML, Kartiko S, Yu W, Merriweather MY, Vogel P, Zambrowicz BP, Finnell RH. Mouse Fkbp8 activity is required to inhibit cell death and establish dorso-ventral patterning in the posterior neural tube. Hum Mol Genet. 2008; 17(4):587–601. [PubMed: 18003640]
51. Yang XM, Trasler DG. Abnormalities of neural tube formation in pre-spina bifida splotch-delayed mouse embryos. Teratology. 1991; 43(6):643–57. [PubMed: 1882355]
52. Zhang, B.; Kirov, S.; Schmoyer, D.; Snoddy, J. Gene Set Analysis Toolkit V2. Vanderbilt University; 2003. http://bioinfo.vanderbilt.edu/webgestalt/option.php
53. Zhang B, Schmoyer D, Kirov S, Snoddy J. GOTree Machine (GOTM): a web-based platform for interpreting sets of interesting genes using Gene Ontology hierarchies. BMC Bioinformatics. 2004; 5:16. [PubMed: 14975175]
54. Zohn IE, Anderson KV, Niswander L. Using genomewide mutagenesis screens to identify the genes required for neural tube closure in the mouse. Birth Defects Res A Clin Mol Teratol. 2005; 73(9):583–90. [PubMed: 15971254]

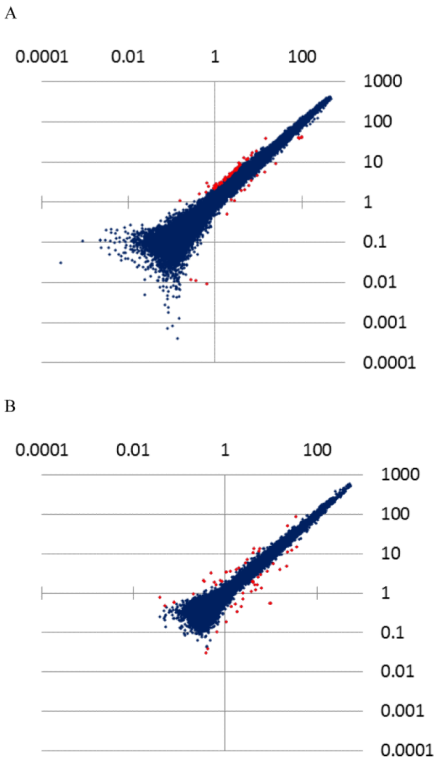

Figure 1.
Scatter plots of the *Fkbp8*$^{+/+}$ vs. *Fkbp8*$^{-/-}$ (A) and *CXL-Sp* +/+ vs. Sp/Sp (B)

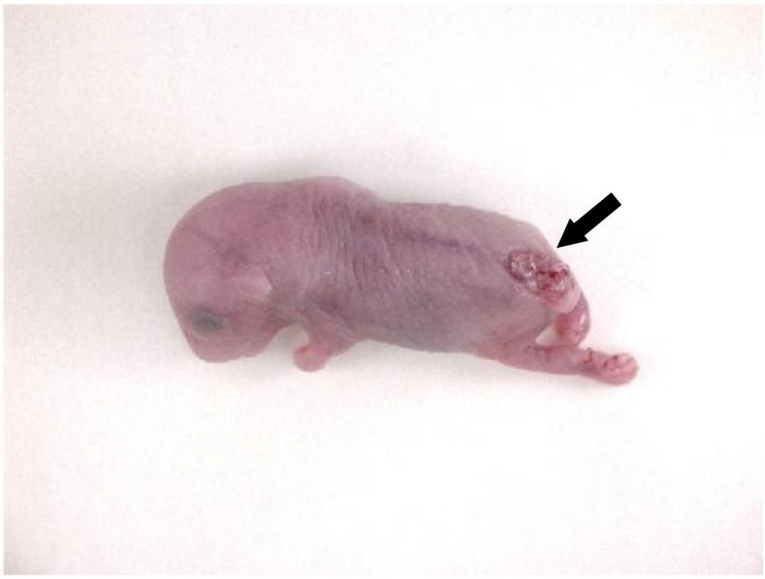

Figure 2.
CXL-Sp (Sp/Sp) fetus (E 18) with spina bifida (arrow) in the lumbo-sacral region.

Figure 3.
Fkbp8$^{-/-}$ fetuses (E18) with spina bifida (arrow) in the thoracico-lumbo-sacral region.

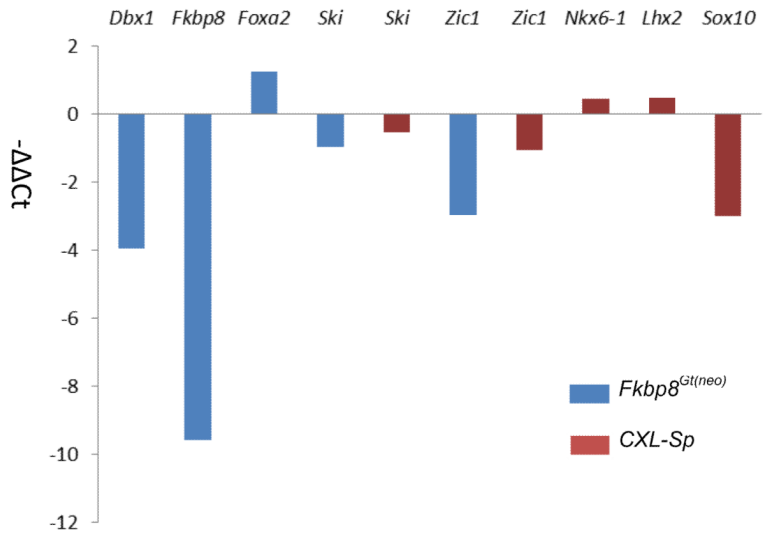

Figure 4.
qRT-PCR: Gene Expression Change of Selected Genes. $-\Delta\Delta Ct$: $\log_2$ (fold change).

Table 1

Gene Ontology Enrichment of Differentially Expressed Genes

A. Enriched gene ontology groups in *CXL-Splotch* gene expression

Mesoderm Development (GO:QQQ7498, N=97), adjusted P=0.0203

Probe_Name	Ratio *	Sp/Sp	+/+	GeneID	Symbol
GE1426782	−1.1	1.78	3.70	226352	*Epb4.1l5*
GE35838	1.0	6.89	3.35	23967	*Osr1*
GE42639	−1.2	0.96	2.19	16870	*Lhx2*

CNS Development (G0:0007417, N=545), adjusted P=0.0203

Probe_Name	Ratio *	Sp/Sp	+/+	GeneID	Symbol
GE33236	−1.9	0.71	2.44	20665	Sox10
GE1480544	1.1	9.46	4.51	18096	Nkx6-1
GE36507	−2.8	0.16	1.05	16814	Lbx1
GE42639	−1.2	0.96	2.19	16870	Lhx2
GE42597	−1.1	3.75	8.22	100044533	Zic1
GE1446602	−1.1	2.03	4.19	13844	Ephb2

B. Enriched gene ontology groups in $Fkbp8^{Gt(neo)}$ gene expression

Dorsal/Ventral Pattern Formation $^{+}$ (G0:0009953, N=91), adjusted P=0.0004

Cell Fate Specification $^{+}$ (G0:0001708, N=75), adjusted P=0.0004

Probe_Name	Ratio *	−/−	+/+	GeneID	Symbol
GE34580	1.1	11.41	5.41	15431	*Hoxd11*
GE35422	1.1	4.16	1.94	15376	*Foxa2*
GE105065	-1.0	2.79	5.74	13172	*Dbx1*
GE36340	−2.7	0.49	3.25	14232	*Fkbp8*

Positive Regulation of Cell Differentiation (G0:0045597, N=489), adjusted P=0.0118

Probe_Name	Ratio *	−/−	+/+	GeneID	Symbol
GE34580	1.1	11.41	5.41	15431	*Hoxd11*
GE35422	1.1	4.16	1.94	15376	*Foxa2*
GE33949	1.1	22.83	10.68	669888	*Lpl*
GE34721	−2.5	0.7	1.85	11486	*Ada*

The values presented in columns: Sp/Sp, +/+ and −/− are normalized median expression level for each gene (CodeLink Expression Analysis software v. 4.0).

[*] The normalized median hybridization signal intensities for mutants were compared to wild types and are presented as the binary logarithm (Log2) ratio for each gene.

[†] The same genes provided enrichment for G0:0009953 and G0:0001708.

Table 2

Real Time Quantitative PCR Results

symbol	strain	Genotype	-ΔΔC_T **	Fold Change	p-value	Microarray ratio **
Dbx1	Fkbp8$^{Gt(neo)}$	−/− *vs* +/+	−3.95	**0.064**	**0.04**	−1.0
Fkbp8	*Fkbp8* $^{Gt(neo)}$	−/− *vs* +/+	−9.58	**0.001**	**0.01**	−2.7
Foxa2	*Fkbp8* $^{Gt(neo)}$	−/− *vs* +/+	+1.24	2.357	0.10	+1.1
Ski	*Fkbp8* $^{Gt(neo)}$	−/− *vs* +/+	−0.96	0.513	0.09	−1.1
Ski	*CXL-Sp*	*Sp/Sp vs* +/+	−0.52	0.697	0.52	−1.0
Zic1	Fkbp$^{8Gt(neo)}$	−/− *vs* +/+	−2.98	**0.127**	**0.02**	−1.0
Zic1	*CXL-Sp* *	*Sp/Sp s* +/+	−1.07	**0.476**	**0.01**	−1.1
Nkx6-1	*CXL-Sp*	*Sp/Sp vs* +/+	+0.44	1.356	0.19	+2.1
Lhx2	*CXL-Sp*	*Sp/Sp vs* +/+	+0.47	1.385	0.56	−1.2
Sox10	*CXL-Sp*	*Sp/Sp vs* +/+	−2.99	**0.126**	**0.0001**	−1.8

* outlier excluded, n=8-12 per genotype

** ΔΔCT and microarray ratio = log2 (fold change). +: increase; −: decrease.